Elevated temperature creep deformation in solid solution strengthened <001> NiAl-3.6Ti single crystals

J. Daniel Whittenberger[1*], Ronald D. Noebe[1] and Ram Darolia[2]

[1] Materials Division, NASA-Glenn Research Center at Lewis Field, Cleveland OH, 44135
[2] GE Aircraft Engines, 1 Neumann Way, Cincinnati, OH, 45215

Abstract

The 1100 to 1500 K slow plastic strain rate compressive properties of <001> oriented NiAl-3.6Ti single crystals have been measured, and the results suggests that two deformation processes exist. While the intermediate temperature/faster strain rate mechanism is uncertain, plastic flow at elevated temperature/slower strain rates in NiAl-3.6Ti appears to be controlled by solute drag as described by the Cottrell-Jaswon solute drag model for gliding $\mathbf{b} = a_0\langle 101\rangle$ dislocations. While the calculated activation energy of deformation is much higher (~480 kJ/mol) than the activation energy for diffusion (~290 kJ/mol) used in the Cottrell-Jaswon creep model, a forced temperature compensated - power law fit using the activation energy for diffusion was able to adequately (> 90 %) predict the observed creep properties. Thus we conclude that the rejection of a diffusion controlled mechanism can not be simply based on a large numerical difference between the activation energies for deformation and diffusion.

* Corresponding author: NASA-Glenn Research Center, MS 24-1, Cleveland, OH 44135, Phone: 216-433-3196, FAX: 216-433-5033, E-mail: J.Daniel.Whittenberger@grc.nasa.gov

Introduction

The effects of elevated temperature solid solution hardening on the mechanical properties of single phase, B2 crystal structure NiAl-based alloys are not well understood. For example it has been shown [1-3] that the addition of 0.05 at % Zr can dramatically strengthen polycrystalline NiAl at lower temperatures/fast strain rates (from ~70 to ~250 MPa at 1100 K - 10^{-5} s^{-1}); however such hardening is not maintained at higher temperatures/lower creep rates, where both NiAl and NiAl-0.05Zr deform at ~10^{-7} s^{-1} under 15 MPa at 1300 K [3]. The best evidence for persistent solid solution hardening of NiAl to date involves Ti additions to single crystals, where Walston, *et al.* [4] found that the stress- rupture properties of Ni-47.5Al-2.5Ti samples were significantly greater than those of NiAl. A subsequent creep study of Ni-47.4Al-2.35Ti single crystals by Kitabjian *et al.* [5] in 1999 indicated that this Ti addition produced a factor of 6 strength enhancement over Ni-50Al when deformed at ~4 x 10^{-7} s^{-1} at 1273 K. Based on mechanical properties and transmission electron microscopy results, they concluded that deformation was controlled by a solute drag mechanism at the highest temperatures and lowest stresses. However in this examination, even though the stress exponent approached 3, they discounted the Cottrell-Jaswon solid solution creep model [6,7], because their measured activation energy for deformation of ~400 kJ/mol was significantly larger than the reported activation energy for lattice diffusion in NiAl (~300 kJ/mol, [8]).

In addition to the NiAl-2.35Ti crystals studied by Kitabjian *et al.* [5], General Electric Aircraft Engines (GEAE) also grew a few higher Ti-content single crystals as part of a larger effort to develop NiAl-based material for advanced gas turbine engines [4,9,10]. One of these crystals, a <001> oriented, nominally NiAl-3.6Ti, was made available to the Glenn Research Center for testing. Creep measurements on this composition, which is well within the nominally 5 at % solid solubility limit for Ti [11], would allow the effects of alloy chemistry to be examined when combined with the results of [5]. This study presents the 1100 - 1500 K compressive creep properties of <001> oriented NiAl-3.6Ti single crystals and compares these values and those of Kitabjian *et al.* [5] to the predictions of the Cottrell-Jaswon solid solution creep model [6,7].

Experimental Procedures

Materials - A section of a NiAl-3.6Ti crystal was obtained from GEAE for machining into small compression samples, where the original crystal, approximately 25 by 40 mm in cross section and about 100 mm long, had been grown by a modified Bridgman technique [4] and then annealed in argon for 50 h at 1583 K to reduce local dendritic segregation. Upon receipt, the section was placed in a goniometer, checked for orientation by the back reflection Laue technique, and appropriately rotated for the machining of <001> oriented compression specimens. Long cylinders slightly over 4 mm in diameter were wire electrodischarged machined (EDM'ed) from the alloy, centerless ground to 4 mm diameter and then EDM sectioned to yield 8 mm long compression samples. Following machining, four randomly selected specimens (~10 % of the machined test coupons) were checked for orientation by the Laue technique which revealed that the orientation along the sample length was nearly <001> (~4, 5, 6 and 6.5° toward the <111>). Alloy chemistry was determined by destructive analysis of several as-machined compression samples, and these analyses indicated that the composition was close to the intended target values: 49.9Ni-46.4Al-3.60Ti (at. %) with a small amount of minor impurities: 0.004Cr-0.0185Cu- 0.0023Fe-0.013Si (at. %).

Compression Testing - The 1100 - 1400 K slow plastic deformation properties at strain rates ranging from 10^{-2} s^{-1} to 10^{-7} s^{-1} were determined by compressing samples in air between solid SiC push bars under constant velocity conditions in an universal testing machine. The autographically recorded load - time charts from the test machine operating at speeds ranging from 2.1×10^{-3} to 2.1×10^{-6} mm/s were converted to true compressive stresses, strains, and strain rates via the offset method and the assumptions that volume is conserved and all plastic deformation occurred in the specimen.

To compliment the constant velocity testing, strength properties in air at strain rates < 10^{-7} s^{-1} between 1100 K to 1400 K and all the compressive properties at 1500 K were measured by constant load compressive creep testing in lever arm creep frames. Creep strain was determined as a function of time through periodic measuments of the relative positions of ceramic push bars applying the force to the specimen. After normalizing the contraction - time results with respect

to the final specimen length, the data were converted into true stresses, strains and strain rates by assuming volume conservation. While most creep specimens were subjected to multiple engineering stress conditions, a few samples were tested under a single load. Steady state creep rates were determined by linear regression techiques applied to the visually selected linear region of the true stress - time data. Such values were then paired to the average true stress applied during the steady state regime.

In addition to providing the strength properties at several stresses, multiple constant load testing allowed examination of transient creep after the majority of test frame play has been removed by the initial load application. For this analysis, instantaneous strain rates were calculated by stepping five data point linear regression analyses through the entire set of strain - time results and then plotting these values as a function of creep strain.

Results and Discussion

Constant Velocity Testing - The 1100 to 1400 K stress - strain curves determined on <001> NiAl-3.6Ti samples are shown in Fig.1 as a function of the approximate imposed strain rate. There is a significant difference in behavior between testing at the two lower test temperatures (Figs. 1(a,b)) and the two higher temperatures (Fig. 1(c,d)). Normally, one expects that the elevated temperature strength will decrease as the strain rate decreases which is the case for <001> oriented NiAl-3.6Ti at 1300 and 1400 K (Figs. 1(c,d)). However at 1100 K (Fig. 1(a)), and to some extent at 1200 K (Fig. 1(b)), the observed strength levels are not greatly influenced by the imposed deformation rate except for the fastest condition. Such an apparent independence between stress and strain rate has not been previously observed in either polycrystalline NiAl [12] or <001> single crystals (Ni-40Al [13] and NiAl-3Ti [5]) at 1100 K, nor was it seen in either <100> NiAl [14] or NiAl-2.35Ti [5] single crystals at 1123 K.

The stress - strain curves denoted by filled symbols in Figs. 1(a,c) are results from near duplicate testing, and they illustrate that the plastic properties of <001> oriented NiAl-3.6Ti are reproducible. While the lower temperature/faster deformation rate tests exhibit continuous, but slow work hardening (Figs. 1(a,b)), testing at higher temperatures/slower deformation rates

resulted continuous flow under a more or less constant stress (Figs. 1(c,d)).

Constant Load Creep Testing - Creep plots resulting from 1100 to 1500 K testing of <001> oriented NiAl-3.6Ti are given in Fig 2 as a function of engineering stress. The multistress curve for 1100 K testing in Fig. 2(a) has been vertically offset by 2 % in order to separate it from the 1200 K result. With respect to this 1100 K creep test, stress was increased after about 500 ks at an engineering stress of 250 MPa and then increased again after an additional ~500 ks at 320 MPa because very low apparent steady state creep rates ($< 2 \times 10^{-9}$ s^{-1}) were being measured.

In general creep in <001> NiAl-3.6Ti between 1100 and 1500 K (Figs 2(a-d)) was normal after the initial loading, where primary creep was followed by a steady state. While stress increases lead to a new secondary creep rate, two types of creep transients were seen after load changes: (1) at 1100 and 1200 K three of the four stress increases were followed by work hardening over a few tenths to several percent strain to steady state as illustrated by Fig. 3(a) and (2) at 1300 and 1500 K all the load changes resulted in a very limited range of work hardening (<0.1 % strain), if any, giving the appearance of an instantaneous transition to the new steady state value (Fig. 3(b)). For comparison, transient stress experiments for <001>NiAl [14] demonstrated work hardening after stress increases at 1313K and 1473 K. While <001> NiAl-2.35Ti [5] also displayed distinct work hardening after stress increases at 1373 K, <111> oriented NiAl-2.35Ti crystals exhibited strain softening after stress increases at 1273 K. All the test conditions and type of transients for the multistress tests on <001> NiAl-3.6Ti are documented in Appendix 1

Strain Rate - Flow Stress - Temperature Behavior - Fig. 4 illustrates the dependency of the true compressive strain rate ($\dot{\varepsilon}$) on true flow stress (σ) and temperature (T). The open symbol data points represent the flow stresses required to produce 3 percent strain as given by the stress - strain diagrams (Fig. 1) which were determined under constant velocity test conditions. The solid symbols indicate steady state creep rates - average stress values from creep testing (Fig. 2). The 1100 to 1400 K results demonstrate a good agreement between the two test methods. Where reasonable, the data were fitted to a temperature compensated - power law relationship (eqn (1)), or its constant temperature version, defined by

$$\dot{\varepsilon} = A\,\sigma^{n}\exp(-Q/(RT)), \qquad (1)$$

where A is a constant, n is the stress exponent, Q is the activation energy for deformation and R is the universal gas constant. The values for A, n, Q and the standard deviations for the stress exponent (δ_n) and activation energy (δ_Q) as well as the coefficient of determination (R_d^2) for each fit are given in Table 1. The curves in Fig. 4 are the result of the linear regression analyses and indicate the range of data utilized for each fit.

Visual examination of the 1100 K $\dot{\varepsilon} - \sigma$ results in Fig. 4 indicate that the constant load creep test data is consistent with the behavior displayed by the stress - strain curves (Fig. 1(a)) for the constant velocity testing below 2×10^{-4} s^{-1}, where the strain rate seems to be nearly independent of the applied stress. This observation was supported by the attempts to fit the constant temperature version of eqn (1) to the data, where the coefficient of determination was 0.21 for strain rates $<2 \times 10^{-4}$ s^{-1}. Although the 1200 K results could be fitted with eqn (1), its R_d^2 was 0.76 (Table 1) indicating that stress alone is not the sole determinate of the 1200 K plastic flow characteristics.

Within the current range of testing, the 1300 to 1500 K data can be separated into two deformation regimes. At faster strain rates a group of 5 points from the 1300 and 1400 K experiments can be reasonably described by eqn (1) with a stress exponent of ~13.2 and an activation energy of about 773 kJ/mol. At slower strain rates four constant velocity data points and 10 constant load creep measurements from 1300 to 1500 K define a regime with a stress exponent of about 3.4 and an activation energy for deformation of ~484 kJ/mol.

The behavior in Fig. 4 and the deformation parameters in Table 1 for <001> oriented NiAl-3.6Ti are in agreement with the observations of Kitabjian, et. al. [5] for <001> oriented NiAl-2.35Ti, where they found (1) a transition from high stress exponents to lower stress exponents with increasing test temperature {for example: n = 11.2 at 1173 K and n = 3.9 at 1523 K} and (2) a decrease in the apparent activation energies for deformation with decreasing stress {Q = ~725 kJ/mol for stresses ranging from 120 to 160 MPa; while Q = ~450 kJ/mol for stresses from 40 to 80 MPa}.

In both [5] and this study, the plastic flow described by high stress exponents or very high activation energies probably involve lower temperature deformation mechanisms which are somewhat dependent of an evolving dislocation structure, as is suggested by work hardening after a stress increase at 1200 K in Fig. 3(a). Deformation in the $n \approx 3.4$, $Q \approx 484$ kJ/mol regime for <001> oriented NiAl-3.6Ti does not appear to be dependent on an evolving microstructure as very little deformation has occurred after the stress increase before the new steady state creep rate was established (Fig. 3(b)). This implies that the existing mobile dislocations reacted almost instantaneously to the stress change; Kitabjian, *et al.* [5] also concluded that dislocation mobility was the dominant factor in NiAl-2.35Ti single crystals, where solid solution Ti was the controlling factor.

Cottrell-Jaswon Creep Model - While Kitabjian, et. al. [5] believed that solute drag, viscous glide was the elevated temperature rate controlling creep mechanism, they ultimately abandoned the Cottrell-Jaswon solute drag controlled creep model [6,7]. This decision was primarily based on calculated Cottrell-Jaswon creep rates which were low due to the their assumed 400 kJ/mol activation energy for diffusion that was derived from their measured activation energy for deformation. They, however, did note that if a 340 kJ/mol activation energy for diffusion was assumed, the calculated Cottrell-Jaswon creep rates would agree with their highest temperature/slowest strain rate results. In view of this latter observation, we decided once again to apply the Cottrell-Jaswon model, with the current best estimates for the terms in the equation,

to calculate creep rates and compare them to the current creep data for <001> NiAl-3.6Ti and Kitabjian's, *et. al.* [5] results for <001> NiAl-2.35Ti.

The Cottrell-Jaswon steady state creep rate, $\dot{\varepsilon}_{CJ}$, [6,7] is given by

$$(\dot{\varepsilon}_{CJ}kT/(D\mu b)) = (1/(3e^2c)) \cdot (kT/(\mu b^3))^2 \cdot (\sigma/\mu)^3 \qquad (2)$$

where k is Boltzmann's constant, D is the volume diffusion coefficient, μ is the temperature dependent shear modulus, b is the magnitude of the Burgers vector, e is the linear solute-solvent size difference, and c is the solute concentration in mole fraction. Following Kitabjian, et. al. [5]

$e = 0.101$ [15]
μ (GPa) = $C_{44}(T) = 113.15 - 0.02631 \cdot (T-273)$, [16]
$c = 0.0235$ for NiAl-2.35Ti or
$c = 0.0364$ for the present NiAl-3.6Ti

As opposed to Kitabjian, et. al.[5], who used the magnitude of a $\mathbf{b} = a_0\langle 001\rangle$ type dislocations in their calculations, we have assumed that $\mathbf{b} = a_0\langle 101\rangle$ are the gliding dislocations in an <001> oriented NiAl crystal [17,18]; thus b in eqn (2) = 0.4077 nm.

The last term, which must be defined, for the use of eqn (2) to estimate strain rates is D. Diffusion in NiAl has been extensively studied through both radioactive Ni tracer [8, 19], binary interdifusion [20-22], and third element interdiffusion [23-25] experiments. Table 2 lists the experimental method, appropriate values for the pre-exponential term, D_0, and the activation energies for diffusion, Q_D, from these studies and the compositions which resulted in minimum rates except for Ti diffusion in NiAl, where the volume diffusion coefficients (m^2/s) as a function of temperature is given by

$$D = D_0 \cdot \exp(-Q_D/(RT)) \qquad (3)$$

Table 3 gives the normalized rates of diffusion between 1100 and 1500 K calculated from the parameters in Table 2, where normalization was accomplished using the Ni tracer diffusion coefficients of Frank *et al.* [19]. This latter table indicates that the measured diffusion

coefficients from seven of the eight studies are quite close to one another, particularly between 1300 and 1500 K, even though there is a ~75 kJ/mole (about 25%) difference among the activation energies for diffusion (Table 2).

Based on the results and analysis in Table 3, the diffusion coefficients determined by Frank *et al.* [19] are representative of atom motion in NiAl and were utilized in the present calculation of the Cottrell-Jaswon creep rates (eqn (2)). This preference was made as Frank's *et al.* measurements [19] were determined in NiAl single crystals from 1051 to 1629 K, while the coefficients from Minamino *et al.* [23-25] were derived from 1423 to 1648 K experiments. Such a choice should give reasonable Cottrell-Jaswon creep rates, as all the other diffusion coefficient equations (Table 2) would give only slightly slower [24,25] or somewhat faster [8,21-23,25] values (Table 3).

The results from the Cottrell-Jaswon creep rate calculations are presented in Fig. 5 along with the flow stress - strain rate - temperature data for <001> oriented NiAl-2.35Ti [5] and NiAl-3.6Ti (Fig. 4), where all the strain rates have been normalized by Frank's activation energy for diffusion (288.5 kJ/mol, Table 2). The agreement shown in this figure between the measured elevated temperature, slow strain rate values for <001> oriented NiAl-2.35Ti (Fig. 5(a)) and NiAl-3.6Ti (Fig. 5(b)) and the model is outstanding. The Cottrell-Jaswon model predictions of the strain rates are within a factor of ~3 of those observed for either alloy and such estimates (eqn (2)) were made without any adjustable parameters. From this calculation and the observation that changes in the steady state creep rate occurred with very little, if any, work hardening and almost instantaneously upon load changes (Fig. 3(b), Appendix 1), we conclude that high temperature, slow strain rate creep in <001> oriented solid solution NiAl-xTi single crystals is the result of solute drag as described by the Cottrell-Jaswon model [6,7].

Activation Energy for Deformation - Clearly the above analyses of elevated temperature deformation in solid solution <001> NiAl-xTi crystals reveals that there is a very large difference between the activation energies determined from the $\dot{\varepsilon}$ - σ - T data itself (Table 1, [5]) and the activation energy for diffusion used to apply the Cottrell-Jaswon model (eqn (2)). Based on the 95% confidence limits for fitting eqn (1), one would expect that the "correct" activation energies

for deformation would be 484 ± 48 kJ/mol for NiAl-3.6Ti (Table 1) and 415 ± 28 kJ/mol for NiAl-2.35Ti [5]. Thus the 288.5 kJ/mol activation energy [19] chosen for normalization should, at least apriori, be unable to collapse the data into a master curve. But as can be seen in Fig. 5, the activation energy of 288.5 kJ/mol [19] utilized for normalization was able to collapse all the experimental high temperature, slow strain rate data for both materials into narrow bands.

This paradox is partially due to the linear regression method which is based on minimizing the error between prediction and experiment. Linear regression does not take "physical meaningfulness" into account when calculating regression parameters; its only concern is a minimum error in reproducing the original results. Basically linear regression techniques reject all combinations of deformation parameters which give good fits in favor of the one combination that gives the best fit. The consequence of this approach can be visualized in Fig. 6, where the goodness of regression fitting (R_d^2) is plotted against activation energy.

These plots were generated from forced linear regression fits of the higher temperature/slower strain rate results for <001> NiAl-2.35Ti (Fig. 5(a)) and NiAl-3.6Ti (Fig. 5(b)) to

$$\dot{\varepsilon}/\exp(-Q/(RT)) = A\,\sigma^{n}, \qquad (4)$$

where Q was forced to range from 200 to over 1000 kJ/mol. As expected, Fig. 6 does certainly indicate that the best choice for Q to predict the data is near 450 kJ/mol for both materials. On the other hand, these graphs indicate that any activation energy between 275 to 750 kJ/mol for NiAl-2.35Ti (Fig. 6(a) and ~250 and 1000 kJ/mol for NiAl-3.6Ti (Fig. 6(b)) will result in a $R_d^2 \geq 0.91$. Thus one has an ~ 500 kJ/mol band for acceptable activation energies in <001> NiAl-2.35Ti and an ~750 kJ/mol band for acceptable activation energies in <001> NiAl-3.6Ti which will account for > 90 % of the dependence of strain rate on stress and temperature.

Due to the behavior illustrated in Fig. 6, one can understand how the 288.5 kJ/mol activation energy for Ni tracer in NiAl [19] was able to collapse the strain rate data in Fig. 5 into master curves, as this activation energy is within the band of allowable activation energies which can successfully (> 90 %) describe the original data. Furthermore with a 288.5 kJ/mol activation

energy being acceptable for both materials, it lend credence to our conclusion that Cottrell-Jaswon creep is the controlling mechanism for elevated temperature, slow plastic deformation in solid solution <001> NiAl-xTi alloys.

In terms of understanding the calculated activation energy for deformation, the implication of Fig. 6 is that fitting experimental data to equations like eqn (1) can not be used to categorically prove that the deformation process is not volume diffusion controlled when there is a significant discrepancy between the activation energy for deformation and activation energy for diffusion. At least for <001> NiAl-xTi samples (Fig. 6) any activation energy between 275 kJ/mol and 700 kJ/mol will acceptably describe the original data. Therefore a more realistic approach would be to assume that the activation energy for deformation is equal to that for volume diffusion and from eqn (3) determine if Q_D can reasonably predict the experimental results. If such a calculation is affirmative, a volume diffusion controlled deformation mechanism has to be considered.

Lastly, the shape of the two Coefficient of Determination as a function of Q curves in Fig. 6 indicates that the use eqn (1) to calculate activation energy for deformation will probably yield a high Q value, rather than low activation energy. This tendency results from the non-symmetrical behavior of the R_d^2 - Q plots, where the ability-to-predict rapidly rises from 275 kJ/mol to a maximum at ~450 kJ/mol and then slowly declines. Thus, in view of the normal expectation of some spread in experimental data and the dependency of Coefficient of Determination on activation energy (Fig. 6), any calculation of $Q = Q_D$ would be fortuitous at best. Since there is nothing unique in the elevated temperature deformation data for <001> oriented NiAl-xTi single crystals, we would expect that most calculations of activation energies for deformation will yield values greater than the activation energy for diffusion.

Intermediate Temperature Deformation - While the elevated temperature creep mechanism has been identified in <001> NiAl-xTi single crystals, the controlling deformation process(es) occurring at lower temperatures has not been resolved. In particular there appears to be a significant effect due to Ti content, as can be seen in Fig. 5. While all the NiAl-2.35Ti results

from 1173 to 1523 K testing can be described by a single smooth band, the lower strain rate data from 1100 and 1200 K experiments on NiAl-3.6Ti crystals define a second, separated group which is distinct from the smooth band comprised of 1300 - 1500 K results and the faster 1100 & 1200 K strain rate data. As both Kitabjian, et. al. [5] study and the current work (Fig. 3(a), Appendix 1) revealed evidence for work hardening following stress increases, an evolving microstructure could be an important factor during intermediate temperature deformation. There are also indications in other solid solution strengthened NiAl <001> crystals that dislocation structure is a dominant factor [26]. Much more effort is needed to understand the behavior at intermediate temperatures of NiAl-xTi crystals.

Summary and Conclusion

The compressive slow plastic strain rate properties of <001> oriented NiAl-3.6Ti single crystals have been determined between 1100 and 1500 K. Analysis of the data suggests that two deformation processes exist. While the intermediate temperature/faster strain rate mechanism is uncertain, plastic flow at elevated temperature/slower strain rates in both <100> NiAl-2.35Ti [5] and NiAl-3.6Ti appears to be controlled by solute drag as described by the Cottrell-Jaswon solute drag model of gliding $\mathbf{b} = a_0\langle 101\rangle$ dislocations. Based on the examination of the ability of temperature compensated power laws to predict the creep properties, we conclude that the rejection of a diffusion controlled mechanism can not be made based on large numerical differences between the activation energies for deformation and diffusion.

Acknowledgment

J.D. Whittenberger and R.D. Noebe would like to acknowledge the financial support of the HOTPC project of the NASA-Glenn Research Enter at Lewis Field. Authors would like to thank S.V. Raj for his insightful review.

References

1. S.V. Raj, R.D. Noebe and R. Bowman, *Scripta Met.* **23** (1989) 2049-54.

2. R.R. Bowman, R.D. Noebe, S.V. Raj and I.E. Locci, *Metal. Trans. A* **23A** (1992) 1493-1508.

3. J.D.Whittenberger and R.D. Noebe, *Met. Mat. Trans. A* **27A** (1996) 2628-41.

4. W.S.Walston, R.D. Field, J.R. Dobbs, D.F. Lahrman and R. Darolia: Structural Intermetallics, (eds. R. Darolia, J.J. Lewandowski, C.T. Liu, P.L. Martin, D.B. Miracle and M.V. Nathal) TMS, Warrendale, PA 1993, pp. 523-532.

5. P.H. Kitabjian, A. Garg, R.D. Noebe and W.D. Nix: *Metal. Mater. Trans. A* **30A** (1999) 587-600.

6. A.H. Cottrell and M.A. Jaswon, *Proc. R. Soc.* **A199** (1949) 104-14.

7. F.A. Mohamed and T.G. Langdon, *Acta Metall.* **22** (1974) 779-88.

8. G.F. Hancock and B.R. McDonnell, phys. Stat. Sol. (a) 4 (1971) 143-150.

9 R. Darolia and W.S. Walston, Structural Intermetallics 1997, (ed. M.V. Nathal, R. Darolia, C.T. Liu, P.L. Martin, D.B. Miracle, R. Wagner and M. Yamaguchi) TMS, Warrendale, PA, 1997, TMS pp. 585-594.

10. W.S. Walston and R. Darolia, Structural Intermetallics 2001, eds. K.J. Hemker, D.M. Dimiduk, H. Clemens, R. Darolia, H. Inui, J.M. Larsen, V.K. Sikka, M. Thomas, J.D. Whittenberger, TMS, Warrendale, PA, 2001 pp. 735-744.

11. R.D. Field, R. Darolia and D.F. Lahrman, *Scripta Metall.* **23** (1989) 1469-74.

12. J.D.Whittenberger, *J. Mat. Sci.* **23** (1988) 235- 40.

13. J.D.Whittenberger, R.D. Noebe, C.L Cullers K.S. Kumar and S. K. Mannan, *Metall. Trans. A.* **22A** (1991) 1595-1607.

14. K.R. Forbes, U. Glatzel, R. Darolia and W.D. Nix, *Metal. Mat. Trans.* A **27A** (1996) 1229-40.

15. P.H. Kitabjian and W.D. Nix, *Acta mater.* **46** (1988) 701-710.

16. N. Rusovic' and H. Warlimont, *phys. stat sol. (a)* **44** (1977) 609-619.

17. R.D. Noebe and A. Garg, NASA TM-106981, August 1995.

18. M.J. Mills, R. Srinivasan and M.S. Daw, *Phil. Mag. A* **77** (1998) 801-23.

19. St. Frank, S.V. Divinski, U. Södervall and Chr. Herzig, *Acta mater.* **49** (2001) 1399-1411.

20. S. Shankar and L.L Seigle, *Met. Trans A* **9A** (1978) 1467-76.

21. S. Kim and Y.A. Chang, *Met. Mater Trans. A*, **31A** (2000) 1591-1524.

22. R. Nakamura, K. Takasawa, Y. Yamazaki, and Y. Iijima, *Intermetallics* **10** (2002) 195-204.

23. Y. Minamino, Y. Koizumi and Y. Inui, *Defect and Diffusion Forum* **194-199** (2000) 517-22.

24. Y. Minamino, Y. Koizumi, N.Tsuji, M. Morioka, K. Hirao, and Y.Shirai, *Sci. Tech. Adv. Mater.* **1** (2000) 237-249.

25. Y. Minamino, Y. Koizumi, N.Tsuji, and S. Yakoyama, *J. High Temperature Society (Japan)*, **28** (2002) 322-27.

26. A. Garg and R.D. Noebe, *Scripta Mater.* **39** (1998) 437-43.

Table Captions

Table 1. Temperature compensated - power law descriptions of the strain rate - flow stress - temperature behavior of <001> NiAl-3.6Ti single crystals

Table 2 Experimental method and descriptive parameters describing diffusion in NiAl determined by several investigators.

Table 3. Estimated relative rates of diffusion in NiAl as a function of temperature normalized with respect to the diffusion rates of Frank *et al.* [19] for Ni tracer.

Appendix 1. Type of creep transient observed following an engineering stress change during constant load creep testing of <001> oriented NiAl-3.6Ti single crystals.

Figure Captions

Figure 1. True compressive stress - strain curves as a function of the nominally imposed strain rate for <001> oriented NiAl-3.6Ti tested at (a) 1100 K, (b) 1200 K, (c) 1300 K and (d) 1400 K.

Figure 2. Constant load creep curves for <001> oriented NiAl-3.6Ti as a function of engineering stress at (a) 1100 and 1200 K, where the 1100 K data is offset by 2%; (b) 1300 K, (c) 1400 K and (d) 1500 K.

Figure 3. Changes in the instantaneous strain rate as a function of creep strain in <001> oriented NiAl-3.6Ti as a result of an increase in the engineering stress. (a) 235 to 288 MPa transition at 1200 K and (b) 5 to 10 MPa transition at 1500 K. In both parts the open squares represent data for the lower stress and the open stars represent data for the higher stress.

Figure 4. True compressive flow stress - strain rate - temperature behavior for <001> oriented NiAl-3.6Ti, where the open symbols represent data from constant velocity testing and the solid symbols are results from constant load creep testing.

Figure 5. Flow stress as a function of normalized strain rate for <001> oriented (a) NiAl-2.35Ti and (b) NiAl-3.6Ti compared to Cottrell-Jaswon solute drag model predictions (eqn (2)) given as the solid curve in each part.

Figure 6. Ability of regression analyses, as measured by the Coefficient of Determination, to predict strain rate – flow stress – temperature properties for <001> oriented (a) NiAl-2.35Ti [5] and (b) NiAl-3.6Ti by forcing values of the activation energy of deformation (eqn (4)).

Table 1. Temperature compensated - power law descriptions of the strain rate - flow stress - temperature behavior of <001> NiAl-3.6Ti single crystals

Temperature Regime	A, s^{-1}	n	δ_n	Q, kJ/mol	δ_Q,	R_d^2
Intermediate temperatures and/or higher strain rate fits						
1200 K	2.84×10^{-82}	31.61	7.29	-	-	0.758
1300 - 1400 K	1.21×10^{-3}	13.22	1.93	772.9	111.9	0.964
Higher temperature - lower strain rate fit						
1300 - 1500 K	4.23×10^{6}	3.39	0.15	484.2	28.0	0.979

Table 2 Experimental method and descriptive parameters describing diffusion in NiAl determined by several investigators.

Type of Experiment	D_0, m^2/s	Q_D, kJ/mol	Composition	Reference
Ni tracer	4.46×10^{-4}	308.2	Ni-50Al	[8]
Ni tracer	2.98×10^{-5}	288.5	Ni-50Al	[19]
Interdifusion	3.81×10^{-6}	233.7	Ni-48Al	[20]
Interdifusion	1.30×10^{-2}	355	Ni-50Al	[21]
Interdifusion	5.50×10^{-2}	365	Ni-47Al	[22]
In in NiAl	2.00×10^{-3}	326	Ni-49.4Al	[23]
Pt in NiAl[1]	6.20×10^{-5}	299.6	Ni-49.7Al	[24]
Ti in NiAl	1.85×10^{-3}	342	Ni-49.7Al	[25]
Ti in NiAl	2.71×10^{-3}	332	Ni-46.9Al	[25]

[1] The D_0's and Q values reported in Table 2 of [24] are actually those for In diffusion in NiAl from [23]; the D_0's and Q for Pt in Ni-49.7Al above were taken from Fig. 7 of [24].

Table 3. Estimated relative rates of diffusion in NiAl as a function of temperature normalized with respect to the diffusion rates of Frank *et al.* [19] for Ni tracer.

	Normalized Ratios							
						Third Elements		
Temperature, K	Ni Tracer	Binary Interdiffusion			In	Pt	Ti (49.7Al)	Ti (46.9Al)
	[8]	[20]	[21]	[22]	[23]	[24]	[25]	[25]
1100	1.74	51.2	0.30	0.43	0.37	0.62	0.18	0.78
1200	2.08	31.0	0.56	0.86	0.57	0.68	0.29	1.16
1300	2.42	20.3	0.93	1.56	0.83	0.75	0.44	1.63
1400	2.76	14.2	1.44	2.58	1.13	0.80	0.63	2.17
1500	3.08	10.4	2.11	4.00	1.49	0.85	0.85	2.78

Appendix 1. Type of creep transient observed following an engineering stress change during constant load creep testing of <001> oriented NiAl-3.6Ti single crystals.

Temperature K	Previous Stress, MPa	New Stress MPa	Type of Transient
1100	250	320	Work hardening
1100	320	391	Work hardening
1200	200	235	Very limited work hardening
1200	235	288	Work hardening
1300	29	47	Very limited work hardening
1500	5	10	Very limited work hardening
1500	7.5	21	Very limited work hardening
1500	21	7.5	Very limited work hardening

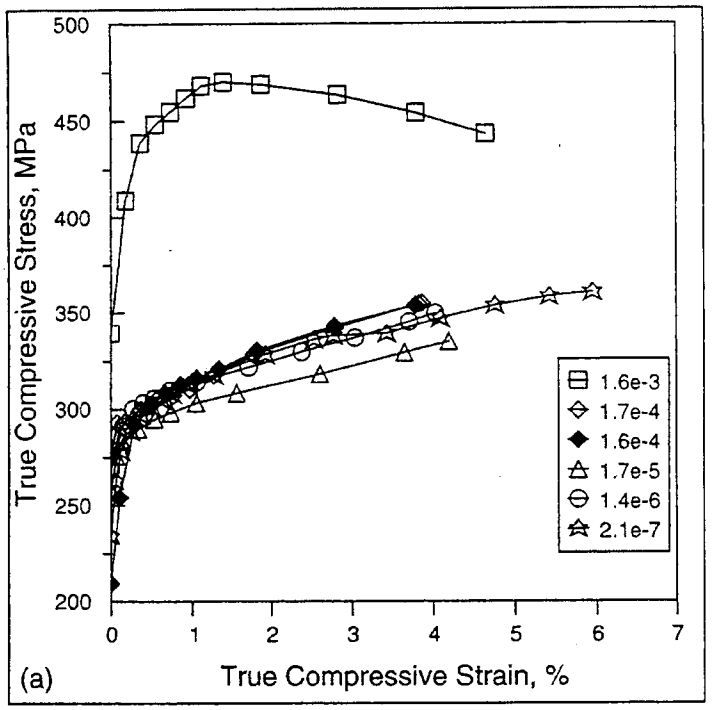
True Compressive Stress, MPa
True Compressive Strain, %
(a)
1.6e-3
1.7e-4
1.6e-4
1.7e-5
1.4e-6
2.1e-7

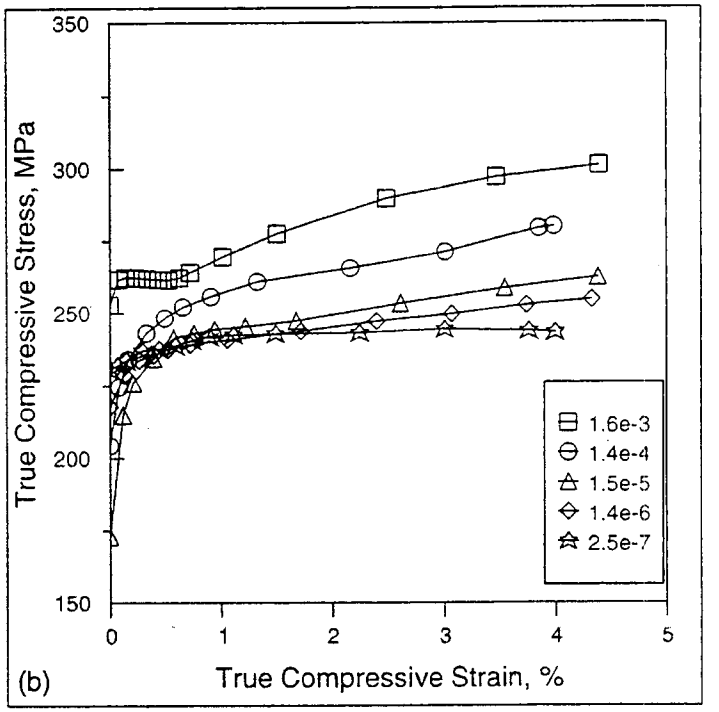
True Compressive Stress, MPa
True Compressive Strain, %
(b)
1.6e-3
1.4e-4
1.5e-5
1.4e-6
2.5e-7

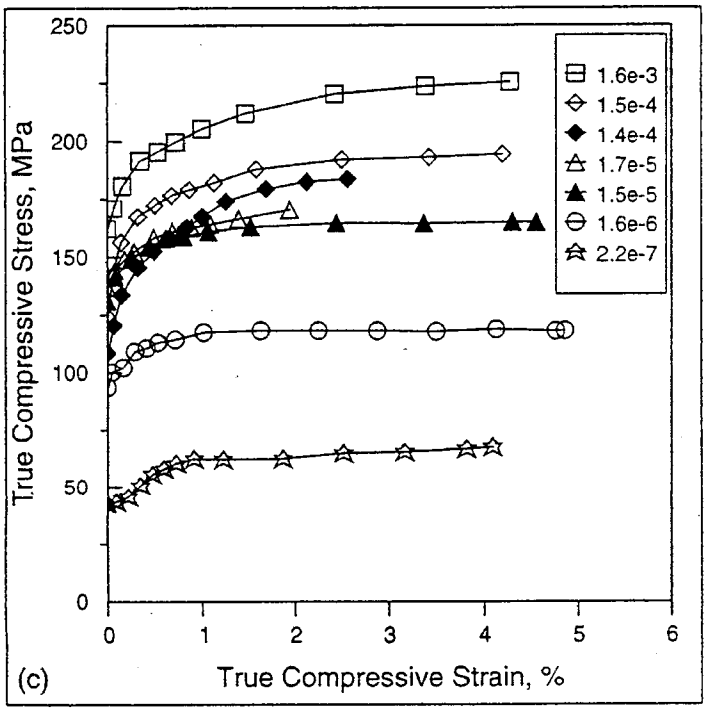
True Compressive Stress, MPa
True Compressive Strain, %
(c)
1.6e-3
1.5e-4
1.4e-4
1.7e-5
1.5e-5
1.6e-6
2.2e-7

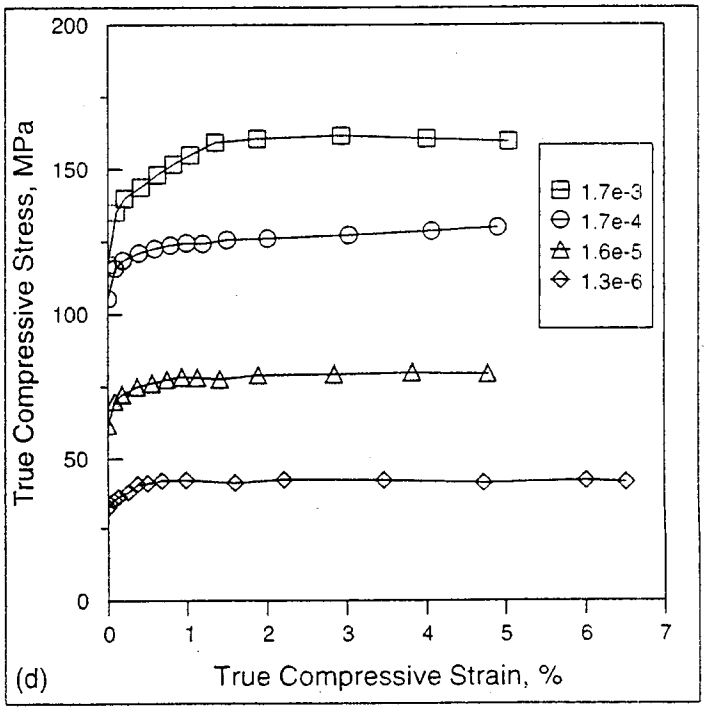
True Compressive Stress, MPa
True Compressive Strain, %
(d)
1.7e-3
1.7e-4
1.6e-5
1.3e-6

Figure 1

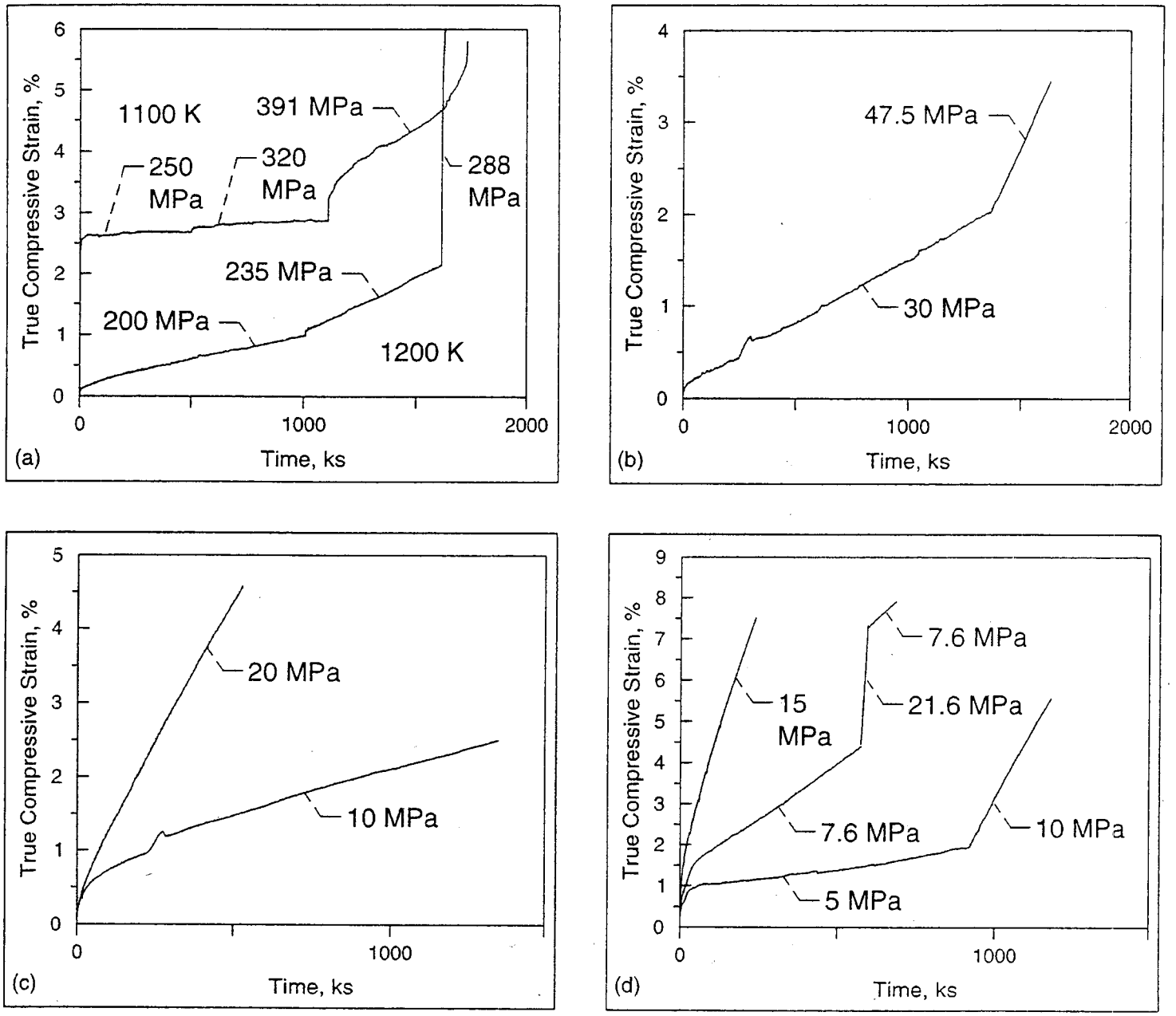
True Compressive Strain, %
Time, ks
(a)
1100 K
391 MPa
250 MPa
320 MPa
288 MPa
235 MPa
200 MPa
1200 K
(b)
47.5 MPa
30 MPa
(c)
20 MPa
10 MPa
(d)
7.6 MPa
15 MPa
21.6 MPa
7.6 MPa
10 MPa
5 MPa

Figure 2

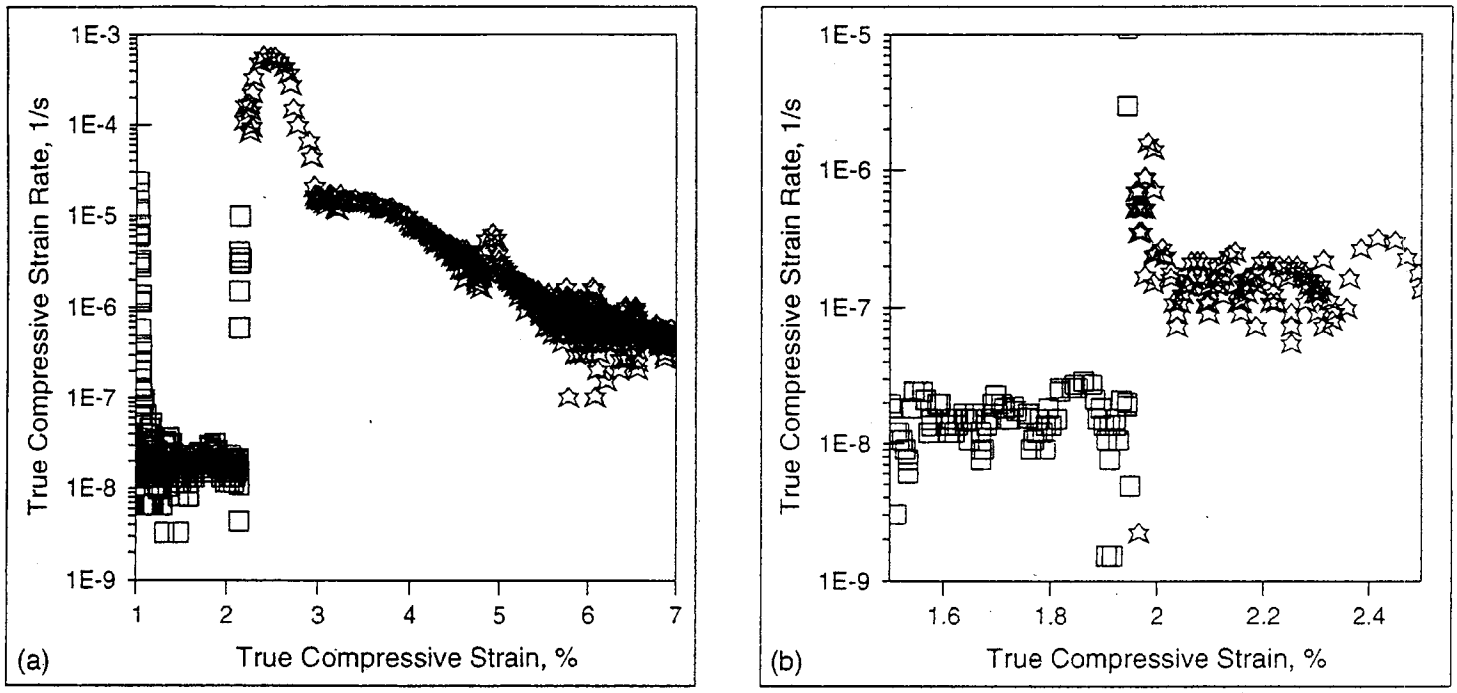
1E-3
1E-4
1E-5
1E-6
1E-7
1E-8
1E-9
True Compressive Strain Rate, 1/s
1
2
3
4
5
6
7
True Compressive Strain, %
(a)
1E-5
1E-6
1E-7
1E-8
1E-9
True Compressive Strain Rate, 1/s
1.6
1.8
2
2.2
2.4
True Compressive Strain, %
(b)

Figure 3

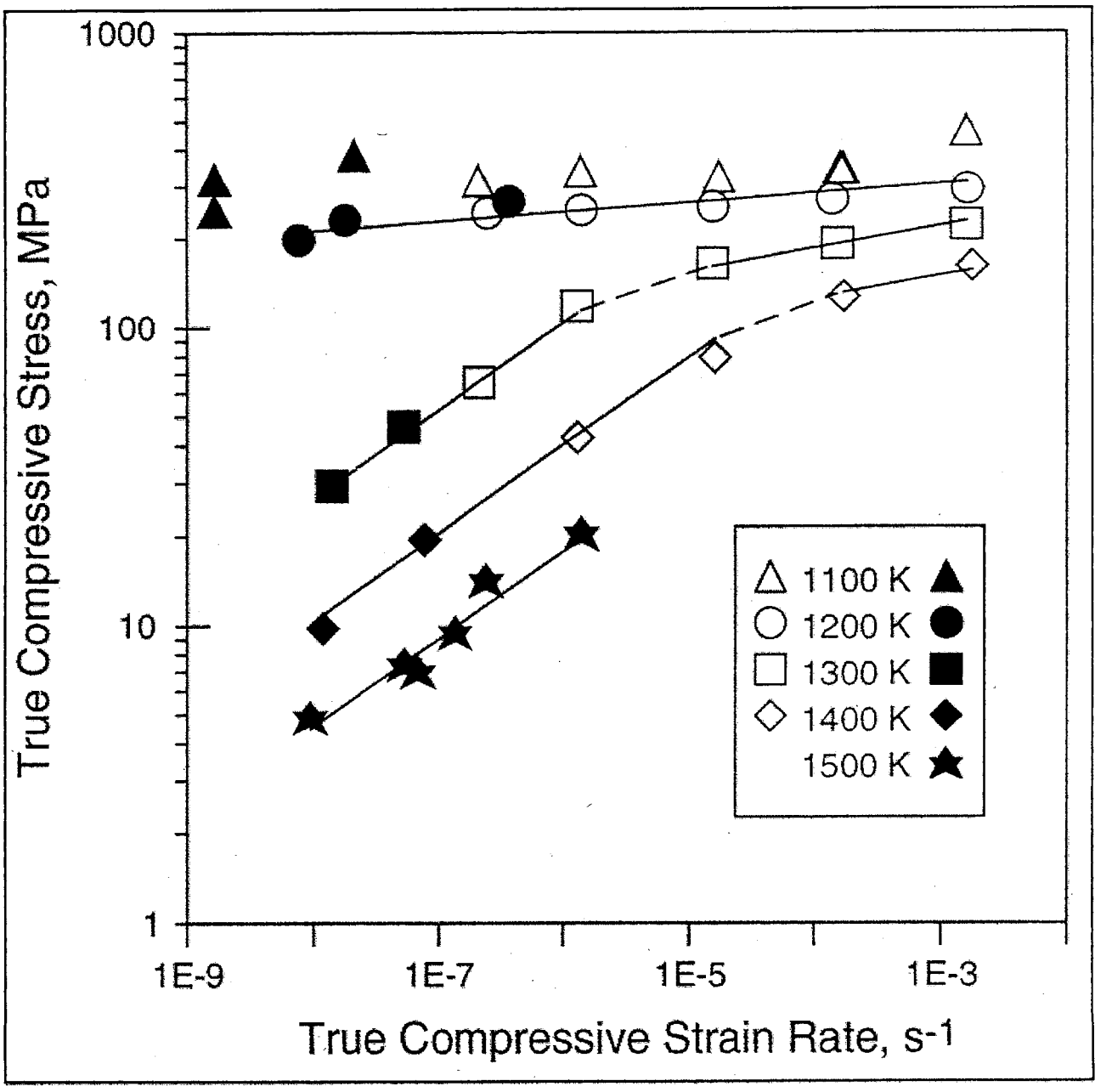
1000
100
10
1
True Compressive Stress, MPa
1E-9
1E-7
1E-5
1E-3
True Compressive Strain Rate, s-1
1100 K
1200 K
1300 K
1400 K
1500 K

Figure 4

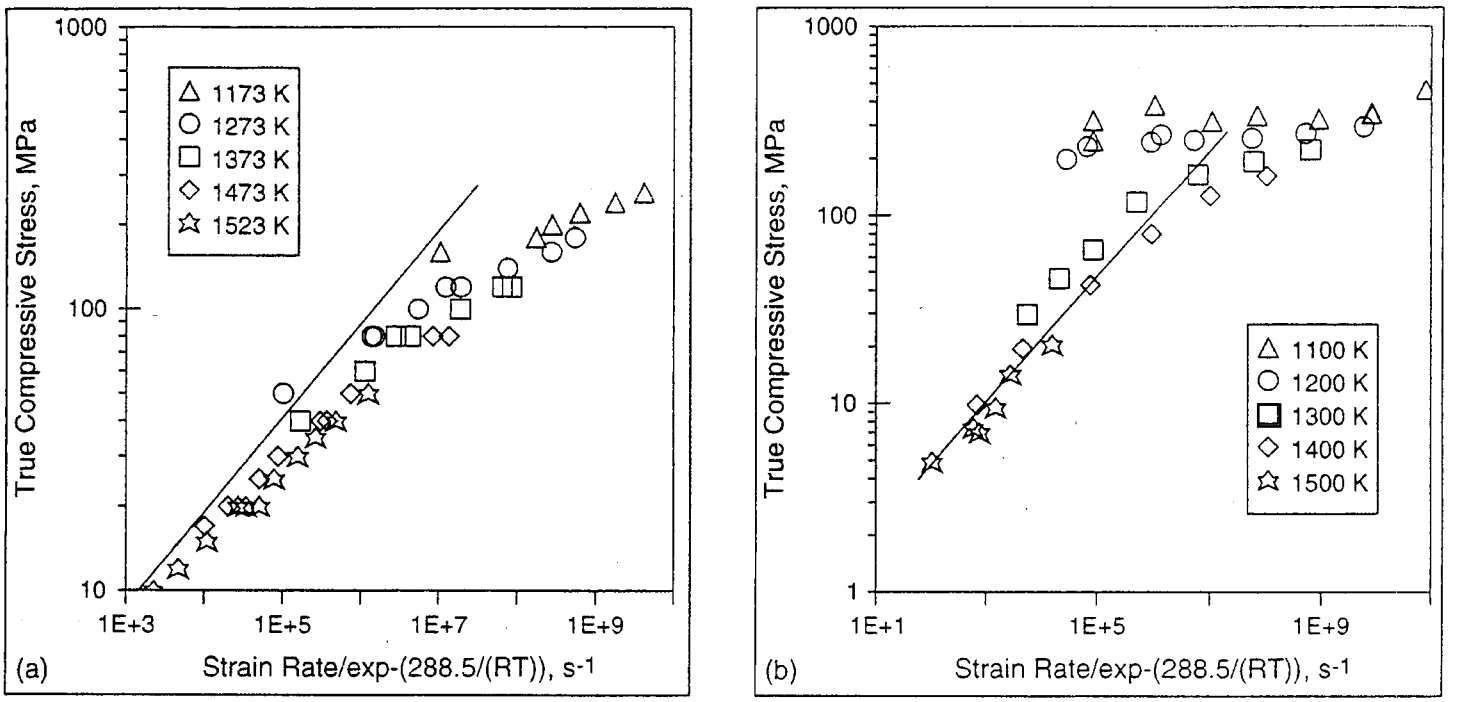
1000
100
10
True Compressive Stress, MPa
1173 K
1273 K
1373 K
1473 K
1523 K
1E+3
1E+5
1E+7
1E+9
(a)
Strain Rate/exp-(288.5/(RT)), s-1
1000
100
10
1
True Compressive Stress, MPa
1100 K
1200 K
1300 K
1400 K
1500 K
1E+1
1E+5
1E+9
(b)
Strain Rate/exp-(288.5/(RT)), s-1

Figure 5

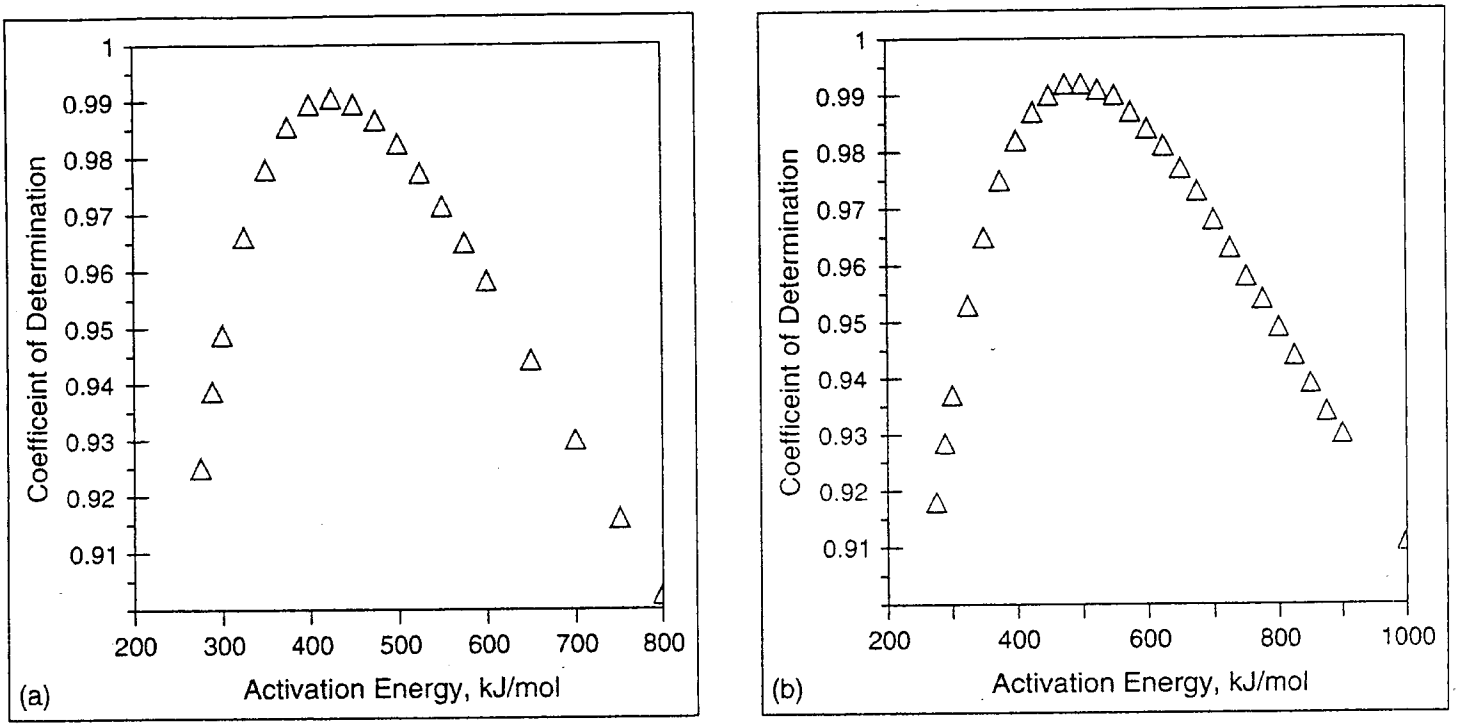
Coefficeint of Determination
1
0.99
0.98
0.97
0.96
0.95
0.94
0.93
0.92
0.91
200
300
400
500
600
700
800
(a)
Activation Energy, kJ/mol
Coefficeint of Determination
1
0.99
0.98
0.97
0.96
0.95
0.94
0.93
0.92
0.91
200
400
600
800
1000
(b)
Activation Energy, kJ/mol

Figure 6